Catalysis Science & Technology

PAPER

Cite this: *Catal. Sci. Technol.*, 2015, 5, 3970

Realization of a highly effective Pd–Cu–Cl_x/Al_2O_3 catalyst for low temperature CO oxidation by pre-synthesizing the active copper phase of $Cu_2Cl(OH)_3$

Xuexun Du,[a] Hui-Ying Li,[a] Jun Yu,[a] Xiuzhen Xiao,[a] Zhangping Shi,[a] Dongsen Mao[a] and Guanzhong Lu*[ab]

Received 14th April 2015,
Accepted 1st June 2015

DOI: 10.1039/c5cy00545k

www.rsc.org/catalysis

The Pd–Cu–Cl_x/Al_2O_3 catalysts (PCC) were prepared by a two-step impregnation (TI) method in organic solvent, wet impregnation (WI) method and NH_3 coordination-impregnation (CI) method. The PCC-TI catalyst prepared by the two-step impregnation method (TI) exhibited much higher activity and stability for CO oxidation than the other catalysts, resulting from the smaller size of $Cu_2Cl(OH)_3$ and fewer carbonates deposited on the surface of PCC-TI catalyst. Using the PCC-TI catalyst, the complete conversion temperature of CO was 10 °C in the presence of 3.1% H_2O. Among the three catalysts, the activation energy (E_a) of PCC-TI/ethanol was the lowest (27.1 kJ mol^{-1}). The PCC-TI/ethanol prepared in ethanol solvent showed a higher activity compared with PCC-TI/methanol, due to much stronger interactions between the copper and palladium species. High concentrations of moisture and CO had a negative effect on the CO conversion. The former is due to excessive numbers of –OH groups (from H_2O dissociation) which occupy the active sites of Pd and Cu, though –OH groups can work as part of the catalytic cycle, and the latter may originate from competitive adsorption and the presence of carbonates on the surface. We used DFT calculations to study the adsorption of H_2O and CO on the surface, and the catalytic cycle of CO oxidation on the Pd species, revealing the possible routes for the formation of common species observed in the *in situ* DRIFTS spectra.

1. Introduction

Low temperature catalytic oxidation of CO has aroused more and more attention because of its wide applications, such as in automotive exhaust purification, room air cleaning and carbon monoxide leak detection.[1–3] Among various catalysts for CO oxidation, the hopcalite catalyst (Cu–Mn mixed oxide) and Co_3O_4 exhibit excellent catalytic activity at room temperature and/or low temperature.[4–6] However, the most frustrating thing is that these catalysts deactivate rapidly in the presence of moisture.[6–8] In the real environment, the moisture content is often closed to saturated-steam at ambient temperature, the susceptibility of the catalysts to water seriously limits their practical application. Nano-gold catalysts have been greatly studied since the pioneering reports by Haruta,[9] and have shown outstanding activity and stability for low temperature CO oxidation even in humid conditions. However, gold nanoparticle catalysts also have some disadvantages, such as sintering of the gold particles, rapid deactivation under halogen-containing atmospheres, the decline of the activity with time on stream, and high cost as a precious metal.[9–12] Hence, research and development of CO oxidation catalysts with high activity and stability is very significant for further practical applications.

The heterogeneous Wacker-type catalyst (supported Pd–Cu–Cl_x) is another attractive catalyst for low temperature CO oxidation, because of its excellent stability in the presence of moisture and halogen compounds, which has been widely researched and reported.[13–22] It is known that $Cu_2Cl(OH)_3$ species play vital roles in supported Pd–Cu–Cl_x catalysts. Lee *et al.* found that the $Cu_2Cl(OH)_3$ phase on the carbon support was a more effective copper species compared with the $CuCl_2 \cdot 2H_2O$ phase, and could reoxidize the reduced palladium species (Pd^0) *via* the Wacker cycle.[16] We have found that in the Pd–Cu–Cl_x/Al_2O_3 catalyst prepared by a NH_3 coordination-impregnation method, the presence of active $Cu_2Cl(OH)_3$ species could enhance the rate determining step from Pd^0 to Pd^+

[a] *Research Institute of Applied Catalysis, School of Chemical and Environmental Engineering, Shanghai Institute of Technology, Shanghai 201418, China. E-mail: gzhlu@ecust.edu.cn; Fax: +86 21 64252923*
[b] *Key Laboratory for Advanced Materials and Research Institute of Industrial Catalysis, East China University of Science and Technology, Shanghai 200237, China*

in the Wacker-type cycle for CO oxidation.[19] In order to achieve the $Cu_2Cl(OH)_3$ active phase, much work has been conducted. For instance, Kim *et al.* investigated the effect of support (as silica, alumina and carbon) on the catalytic properties, and found silica was a less active support compared with alumina and carbon, because the active copper species of $Cu_2Cl(OH)_3$ could not be stabilized on a silica support.[14] Park and Lee used carbon pretreated with HNO_3 as the support for this catalyst due to the enrichment of the carboxylic and carbonyl groups on its surface, and $Cu(NO_3)_2$ as a copper precursor to prepare this catalyst, which helped the formation of the $Cu_2Cl(OH)_3$ phase.[17] Up to now, research has mainly focused on the influence of the support and precursor on the formation of the active $Cu_2Cl(OH)_3$ phase, but directly using the pre-synthesized $Cu_2Cl(OH)_3$ phase to prepare the Pd–Cu–Cl_x/Al_2O_3 catalyst has not been reported yet. In this paper, the active copper phase of $Cu_2Cl(OH)_3$ was synthesized on its own, and then supported on the Al_2O_3 surface to prepare the bimetallic catalyst with excellent activity and stability for room temperature CO oxidation even in the presence of high concentrations of moisture.

Herein, Pd–Cu–Cl_x/Al_2O_3 catalysts were prepared by a two-step impregnation method with different solvents, and their physicochemical and catalytic properties for low temperature CO oxidation were studied to understand the effect of the active copper phase on the catalytic performance. Based on the experimental results, the influence of the physicochemical properties of the catalysts on their catalytic performances, kinetic characteristics, surface reaction *etc.* were discussed in detail. While we used DFT calculations[23] to study the adsorption of H_2O and CO on the surface, and the catalytic cycle of CO oxidation on the Pd species, to reveal the possible routes for the formation of common species observed in the DRIFTS spectra.

2. Experimental section

2.1. Catalyst preparation

$CuCl_2$ (AR), methanol (AR), ethanol (AR) and propylene oxide (AR) were purchased from Sinoharm Chemical Reagent Co., Ltd.; $PdCl_2$ (AR) was purchased from Adamas Reagent Co., Ltd., and Al_2O_3 (WHA-204, BET surface area of 194 m^2 g^{-1}) was purchased from Wenzhou Jingjing Aluminum Ltd.

A 1.7 wt.% Pd–3.3 wt.% Cu–Cl_x/Al_2O_3 catalyst was prepared by a two-step impregnation (TI) method. Firstly, $Cu_2Cl(OH)_3$ was synthesized by a reported method:[24] weighed $CuCl_2$ was dissolved in a 2 mL mixed solution of propylene oxide and alcohol (methanol or ethanol) (volume ratio of propylene oxide/alcohol was 1/1), a pale green turbid liquid was formed after 10 min of adding $CuCl_2$. Then 1 g of Al_2O_3 was impregnated in this solution. After being aged for 24 h, the $Cu_2Cl(OH)_3$/Al_2O_3 sample was dried at room temperature and calcined at 300 °C for 4 h.

Weighed $PdCl_2$ was dissolved in 2 mL of 0.1 M hydrochloric acid, and then the $Cu_2Cl(OH)_3$/Al_2O_3 sample was impregnated in this $PdCl_2$ solution and dried at 25 °C for 12 h. This 1.7 wt.% Pd–3.3 wt.% Cu–Cl_x/Al_2O_3 catalyst sample was denoted as PCC-TI/methanol or PCC-TI/ethanol.

This Pd–Cu–Cl_x/Al_2O_3 catalyst was also prepared by the conventional wet impregnation method in water, and an NH_3 coordination–impregnation method in isopropanol, and were denoted as PCC-WI and PCC-CI, respectively.

2.2. Catalyst characterization

The actual content of Cu and Pd in the catalysts was measured by inductively coupled plasma optic emission spectrometry (ICP-OES) on a PerkinElmer Optima 7000 DV instrument. The surface areas of the samples were measured by N_2 adsorption at −196 °C on a Micrometrics ASAP 2020 M + C adsorption apparatus and calculated by the Brumauer–Emmett–Teller (BET) method. The X-ray powder diffraction (XRD) patterns of the catalysts were performed on a PANalytical X'Pert Pro MRD X-ray diffractometer with CuKα radiation (λ = 0.154056 nm) operated at 40 kV and 40 mA. The mean crystalline sizes of the Cu species in the catalysts were estimated by the Scherrer equation on the basis of the broadening of diffraction peaks.

Hydrogen temperature-programmed reduction (H_2-TPR) of the sample was tested in continuous-flow apparatus equipped with a TCD detector. 100 mg of catalyst was packed in the quartz micro-reactor and pretreated with a N_2 flow of 30 mL min^{-1} at 30 °C for 0.5 h. Then the sample was heated up to 500 °C at 10 °C min^{-1} in a gaseous mixture of 10% H_2/N_2 (30 mL min^{-1}).

The *in situ* diffuse reflectance infrared Fourier transform spectroscopy (DRIFTS) spectra were obtained at room temperature on a Nicolet 6700 FT-IR spectrometer equipped with a MCT detector, in which the spectral resolution was 4 cm^{-1} and scan number was 64 cycles. The DRIFTS cell (Harrick) was fitted with CaF_2 windows and a heating cartridge that allowed samples to be heated to 400 °C. The sample was pretreated in N_2 (50 mL min^{-1}) at 25 °C for 1 h, then the background spectrum was collected in a N_2 atmosphere. After the reactant gas of 0.15% CO–20% O_2–3.1% H_2O/balanced N_2 (50 mL min^{-1}) flowed through the sample cell, the IR absorption spectra on the catalysts were recorded at 25 °C.

2.3. Computational details of DFT study

The DFT calculations were performed with the help of the Vienna *ab initio* simulation package (VASP) code. The generalized gradient approximation (GGA) was used to solve the Kohn–Sham equations. The project-augmented wave (PAW) method was adopted to represent the core–valence interaction.[25] Like the model used by Digne *et al.*,[26] herein, the optimized lattice parameters of γ-Al_2O_3 were taken as a = 5.57, b = 8.39, c = 8.05, and β = 90.598, and the (100) facet was selected as the calculation model, in which a 6-layer slab model contained 24 Al_2O_3 units and the vacuum region between the slabs was set to 16 Å. The valence electronic states were expanded in plane wave basis sets with an energy cut-off at 450 eV. The force threshold for the optimization

and transition state search was 0.05 eV $Å^{-1}$. Only the top two atomic layers of the slab and their adsorbates were allowed to relax, that is to say, the bottom 4 layers were fixed. A $p(1 \times 2)$ surface cell with $1 \times 1 \times 1$ k-point mesh with an area of 11.17×8.41 $Å^2$ was used to fully take the relaxation effects into account. Two criteria were used for searching the transition states by using a constrained optimization scheme: (a) all forces on atoms disappeared, and (b) the total energy was a maximum along the reaction coordination but a minimum with regard to the remaining degrees of freedom.

2.4. Testing of the catalyst performance and kinetic characters

The performances of the catalysts for CO oxidation were tested in a quartz tubular U-tube fixed-bed reactor (Ø5 mm). The sample (200 mg, 20–40 mesh) was packed in the reactor with quartz wool at both sides of the catalyst. A mixture of 1500 ppm CO/air was used as the reactant gas, and its flow rate was 50 mL min^{-1}, corresponding to the weight hour space velocity (WHSV) of 15 000 (mL g^{-1} h^{-1}). Before entering the reactor, the feed gas flowed through a water vapor saturator. The water concentration in the reactant gas could be adjusted from 0.6% to 3.1% by changing the temperature of the water vapor saturator. The CO concentration was monitored by an online gas chromatograph equipped with a FID detector, in which a methanizer was used for hydrogenating CO_2 and CO to methane. The CO conversion was tested after 10 min of reaction. The CO conversion was calculated as X (%) = $(CO_{inlet} - CO_{outlet})/CO_{inlet} \times 100\%$, where CO_{inlet} is the initial CO concentration in the inlet, and CO_{outlet} is the CO concentration in the outlet.

The kinetic data was measured in the same reactor as the catalytic performance testing. Based on the differential reactor mode, the CO conversion was controlled below 15%. The reactant gas consisted of 1500 ppm CO + 3.1% H_2O/air. After steady operation for 30 min, the reaction rates were determined. The oxidation rate of CO was calculated as r (mol g^{-1} h^{-1}) = $(N_{CO} \times X)/W_{cat}$, where N_{CO} is the CO flow rate (mol h^{-1}), W_{cat} is the catalyst weight (g), and X is the CO conversion (%). When the CO conversion was <15%, the influence of the produced CO_2 and H_2O on the reaction rate (r) might be ignored; hence, the empirical equation of the reaction rate for CO oxidation could be measured by eqn (1).

$$r = A\exp\left(-\frac{E_a}{RT}P_{CO}^{\alpha}P_{O_2}^{\beta}\right) \quad (1)$$

A is the preexponential factor; R is the ideal gas constant; T is the reaction temperature; P_{CO} is the partial pressure of CO; P_{O_2} is the partial pressure of O_2.

Taking the logarithm of eqn (1), eqn (2) can be obtained.

$$\ln r = \ln A + \alpha \ln P_{CO} + \beta \ln P_{O_2} - E_a/RT \quad (2)$$

In the process of kinetics data testing, the composition of the reactant gas remained essentially unchanged, and the CO conversion was <15%, therefore, $\ln A$, $\alpha \ln P_{CO}$ and $\beta \ln P_{O_2}$ could be regarded as approximately constant, and eqn (2) can be simplified to $\ln r = -E_a/RT + C$. The activation energy (E_a) can be obtained from the slope of the resulting linear plot of $\ln r$ *versus* $1/T$.

3. Results and discussions

3.1. Influence of preparation method on the catalytic activity and stability

Fig. 1 shows the influence of the preparation method on the catalytic performance of the Pd–Cu–Cl_x/Al_2O_3 catalysts for CO oxidation (1500 ppm CO and ~3.1% water/air). As shown in Fig. 1A, the CO conversion over the PCC-WI catalyst prepared by the wet impregnation method reached a maximum (~83%) at 20 °C, and then decreased with an increase in the reaction temperature, because of the loss of water and chlorine at relatively high temperatures during the reaction.[27] For the other three Pd–Cu–Cl_x/Al_2O_3 catalysts prepared by NH_3 coordination–impregnation and the two-step impregnation method, the PCC-TI/ethanol exhibited a higher catalytic activity: CO was completely converted at 20 °C (T_{100}) over the PCC-CI or PCC-TI/methanol, and T_{100} over PCC-TI/ethanol was only ~10 °C.

The catalytic stability during CO oxidation was also investigated at 25 °C and the reactant gas was 1500 ppm CO and ~3.1% water/air, and the results are shown in Fig. 1B. For the PCC-WI catalyst, the CO conversion was only ~83% after 2 h of reaction, and decreased to ~30% after 10 h. For the PCC-CI catalyst, the CO conversion could be maintained at ~93% for 2 h, and then decreased to ~43% after 10 h. When the two-step impregnation method was employed to prepare the Pd–Cu–Cl_x/Al_2O_3 catalyst, its catalytic stability improved significantly. For the PCC-TI/methanol catalyst, the CO conversion could be maintained above 90% for 22 h of reaction. Using the PCC-TI/ethanol catalyst, the CO conversion remained relatively unchanged after 30 h of reaction at above 93%.

3.2. Influence of moisture on CO catalytic oxidation

The PCC-TI/ethanol catalyst was used as a model catalyst to investigate the influence of moisture on CO catalytic oxidation at 25 °C. As shown in Fig. 2, in the presence of ~0.6% moisture, the catalytic activity of PCC-TI/ethanol remained above 93% for 100 h. In the presence of ~3.1% moisture, its catalytic activity was unchanged for 30 h, and then gradually decreased from ~93% to ~58% CO conversion within 30 h.

These results clearly show that, in the presence of a relatively high concentration of moisture, the catalytic oxidation of CO would be inhibited, that is to say, the catalyst would be deactivated. To further understand this phenomenon, theoretical calculation with DFT for water adsorption and dissociation on the dry γ-Al_2O_3 (100) facet was performed. Structures and an energy diagram of the adsorbed H_2O (IM), transition state for H_2O dissociation (TS) and dissociated H_2O (FS) are shown in Fig. 3. We can see that IM was dissociated through a TS with a small energy barrier (0.10 eV), indicating that the

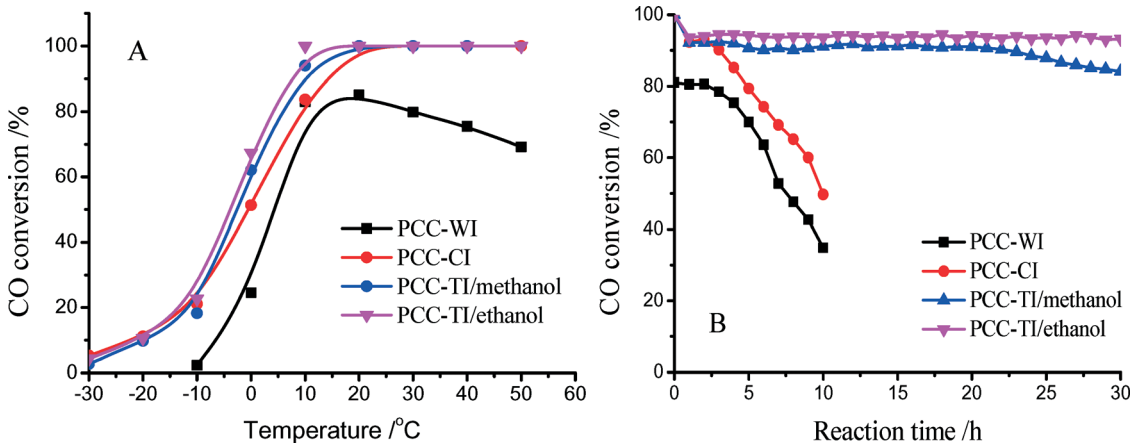

Fig. 1 Influence of the preparation method on the catalytic performance of the Pd–Cu–Cl_x/Al_2O_3 catalysts for CO oxidation in 1500 ppm CO and ~3.1% moisture/air at 25 °C.

formation of the hydroxylated (100) facet of γ-Al_2O_3 is kinetically favored. In this way, the presence of excess H_2O would easily dissociate to –H and –OH, which can occupy the active sites of Pd and Cu on the Al_2O_3 surface as a poisonous species, resulting in a deactivation of the Pd–Cu–Cl_x/Al_2O_3 catalyst for CO oxidation.[7,21] However, the negative effect of the excess of H_2O does not mean that water is dispensable in this process of low-temperature CO oxidation. On the contrary, the proton –H at the O_{3c} site and –OH group at the Al_{5c} site which are dissociated from a certain amount of H_2O, can work as parts of the catalytic cycle as an important species for low temperature CO oxidation over the Pd–Cu–Cl_x/Al_2O_3 catalyst.[23,28]

3.3. Influence of CO concentration on CO catalytic oxidation

Fig. 4 shows the influence of CO concentration on CO oxidation over the PCC-TI/ethanol catalyst at 25 °C. The results show that ~89% CO conversion could be maintained after 30 h of reaction when 750 ppm CO was used; when the CO concentration was increased from 750 ppm to 1500 ppm, the CO conversion increased from ~89% to ~94% and was maintained after 30 h of reaction; when the CO concentration reached 3000 ppm, ~95% CO conversion could only be maintained for 5 h, and then CO conversion gradually decreased from ~95% to ~80% in the following 25 h.

The above results clearly demonstrate the negative influence of a relatively high CO concentration on CO oxidation over the PCC-TI/ethanol catalyst. When the CO concentration was increased from 750 ppm to 1500 ppm, the CO conversion increased gradually, and when the CO concentration continually increased to 3000 ppm, more CO could react with oxygen to form surface carbonates which remained on the surface without timely decomposition to gaseous CO_2. Over the Pd–Cu–Cl_x/Al_2O_3 catalyst, CO_2 could only form carbonates on the acidic Al_2O_3 surface, and cover the active sites or block the pores.[22] Hence, the covering of carbonates and the competitive adsorption between CO and CO_2 on the catalyst surface might be the main reasons for the negative influence of the relatively high CO concentration on the catalytic oxidation of CO.

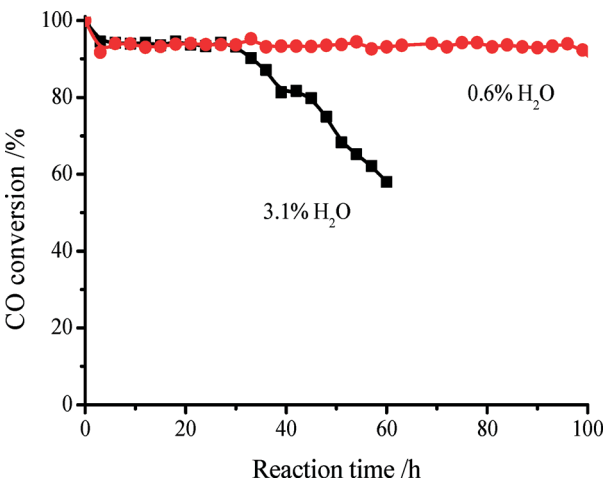

Fig. 2 CO conversion over the PCC-TI/ethanol catalyst in 1500 ppm CO and 0.6 or 3.1% moisture/air at 25 °C.

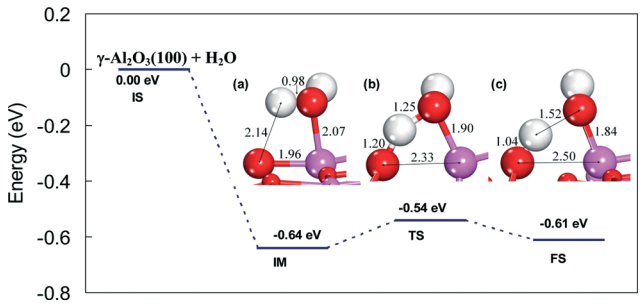

Fig. 3 The energy change and corresponding structures for H_2O dissociation (–H_2O → –H + –OH) on the Al_2O_3(100) facet. (a) Structure of adsorbed H_2O; (b) transition state for H_2O dissociation; (c) structure of dissociated H_2O. (The unit of bond length is Å. O atoms are red, Al atoms are pink, and H atoms are white).

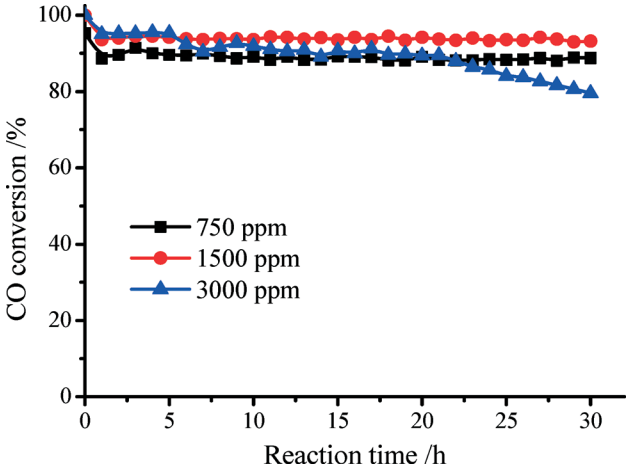

Fig. 4 Influence of the CO concentration on CO oxidation over the PCC-TI/ethanol catalyst at 25 °C with ~3.1% moisture/air.

3.4. Reaction kinetic characteristics

To further understand the effect of the preparation method of the catalyst on its kinetic characteristics for CO oxidation, the apparent activation energies (E_a) for CO oxidation were calculated based on the Arrhenius plots of ln r *versus* $1/T$ (K) (Fig. 5), in which the reactant gas of 0.15% CO–3.1% H_2O/air was used. The reaction rates (r) were tested at differential reactor model with a CO conversion of <15%. As shown in Fig. 5, the value of E_a over the PCC-WI catalyst was 39.8 kJ mol^{-1}, much higher than that over the PCC-CI (29.8 kJ mol^{-1}) and PCC-TI/ethanol (27.1 kJ mol^{-1}) catalysts. Among the E_a values for the three catalysts, that over PCC-TI/ethanol was the lowest. It clearly indicates that the PCC-TI/ethanol catalyst prepared by the two-step impregnation method is the best catalyst for low temperature CO oxidation, compared with PCC-WI and PCC-CI. That is to say, the preparation method has a significant influence on the catalytic performance of the Pd–Cu–Cl_x/Al_2O_3 catalyst by varying the reactivity of the catalyst's active sites or its kinetic behaviour.

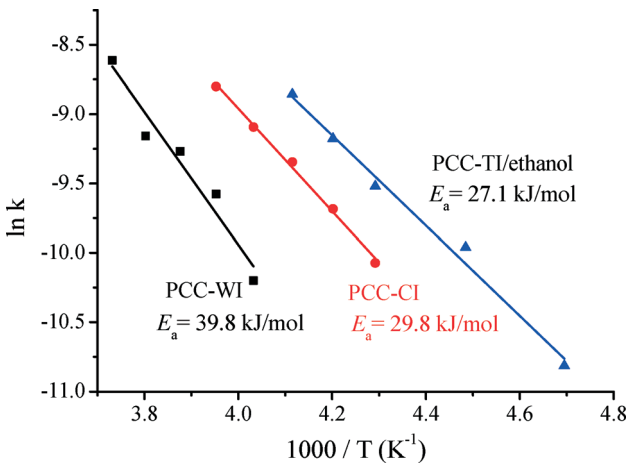

Fig. 5 Arrhenius plots of ln r *versus* $1/T$ over the Pd–Cu–Cl_x/Al_2O_3 catalysts for CO oxidation under 1500 ppm CO and ~3.1% moisture/air.

3.5. Catalyst characterization

XRD and FT-IR tests of pre-synthetized $Cu_2Cl(OH)_3$ species. To evidence that the $Cu_2Cl(OH)_3$ phase was pre-synthetized successfully, the XRD and FT-IR spectra of pre-synthesized $Cu_2Cl(OH)_3$ were tested and are shown in Fig. 6, and are similar to existing reports.[24] In the FT-IR spectrum of $Cu_2Cl(OH)_3$ (Fig. 6A), the two absorption peaks at 3447 and 3358 cm^{-1} are ascribed to the hydroxyl stretching modes $\nu_1(O_1–H_1)/\nu_1(O_{2/3}–H_{2/3})$ of the $Cu_2Cl(OH)_3$, the peaks at 988–923 cm^{-1} are related to the δ_1(Cu–O–H) modes, and signals corresponding to the Cu–O related modes ν_s(O–Cu–O) and ν_1(O–Cu–O) were observed at 587 and 516 cm^{-1}, respectively. In the XRD pattern of $Cu_2Cl(OH)_3$, the five main diffraction peaks at 2θ = 16.19°, 30.95°, 39.75°, 50.46° and 53.75° are indexed to the peaks of chinoatacamite $Cu_2Cl(OH)_3$ (JCPDS 50-1559). Based on the results of FT-IR and XRD measurements, it can be confirmed that the $Cu_2Cl(OH)_3$ has been synthesized successfully.

The $Cu_2Cl(OH)_3$/Al_2O_3 samples with different Cu loadings were prepared by the impregnation method and calcined at 300 °C, and their FT-IR spectra are shown in Fig. 7. Unlike the IR spectrum of pure Al_2O_3 (Fig. 7a), the absorption peaks at 3447 and 3358 cm^{-1} in the IR spectra of $Cu_2Cl(OH)_3$/Al_2O_3 samples are ascribed to the hydroxyl stretching modes $\nu_1(O_1–H_1)/\nu_1(O_{2/3}–H_{2/3})$ of the $Cu_2Cl(OH)_3$. When the Cu loading was 3.3 wt.% (Fig. 7b), the intensities of the absorption peaks at 3447 and 3358 cm^{-1} were very weak, and when the Cu loading was increased from 3.3 wt.% to 13.2 wt.%, the intensities of these two absorption peaks increased gradually. These results show that $Cu_2Cl(OH)_3$ on Al_2O_3 survived after the impregnation and 300 °C calcination.

ICP-OES and BET surface area. Table 1 presented the compositions of Pd and Cu in the catalysts, and the Pd content was ~1.6 wt.% and the Cu content was ~3.2 wt.% for the four samples, which were close to 1.7 wt.% Pd and 3.3 wt.% Cu in the synthesis solution. These results showed that Cu and Pd were perfectly supported on the Al_2O_3 surface by the WI, CI and TI methods.

Compared with the surface area (194 m^2 g^{-1}) of the Al_2O_3 bare support, the surface areas of PCC-WI, PCC-CI and PCC-TI decreased after supporting Pd and Cu components, which may result from the partial blocking of the pores of Al_2O_3 by the Pd and Cu species. The BET surface area of PCC-TI/methanol was 137 m^2 g^{-1}, close to that of PCC-TI/ethanol (139 m^2 g^{-1}), which indicated that the surface area of the PCC-TI catalysts were insignificantly influenced by the organic solvent.

XRD analysis. As shown in Fig. 8, in the XRD patterns of the four Pd–Cu–Cl_x/Al_2O_3 catalysts, only the diffraction peaks of the alumina support and $Cu_2Cl(OH)_3$ could be observed. The diffraction peaks of Pd species were hardly discerned in the all samples, which indicated a high dispersion of Pd

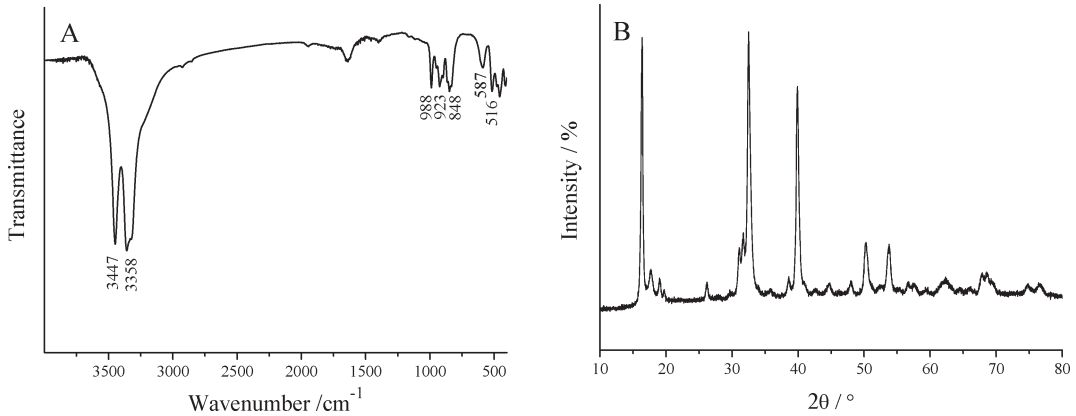

Fig. 6 (A) FTIR and (B) XRD spectra of pre-synthetized $Cu_2Cl(OH)_3$.

species on the alumina or that the content was below the detection limit of XRD. The diffraction peaks of $Cu_2Cl(OH)_3$ species, the active copper phase in Pd–Cu–Cl_x/Al_2O_3, could be observed clearly in the all samples. The mean crystalline sizes of $Cu_2Cl(OH)_3$ are shown in Table 1. Compared with the size (34 nm) of the $Cu_2Cl(OH)_3$ species in the PCC-WI catalyst, its size in the PCC-CI and PCC-TI catalysts was smaller. For example, the one in the PCC-CI catalyst was 16 nm, and those in the PCC-TI/methanol and PCC-TI/ethanol catalysts were 19 nm and 17 nm, respectively. The results above show that different preparation methods can obviously affect the dispersion of the $Cu_2Cl(OH)_3$ phase in the Pd–Cu–Cl_x/Al_2O_3 catalyst or its size, for instance, the X-ray diffraction peaks of $Cu_2Cl(OH)_3$ in the PCC-TI and PCC-CI samples were weaker and broader, indicating that its dispersion in PCC-CI and PCC-TI were higher than that in the PCC-WI catalyst. The high catalytic activity of the PCC-TI samples could be attributed to the smaller size of their $Cu_2Cl(OH)_3$ active phase.[19]

H_2-TPR experiment. In the TPR profile of the $PdCl_2/Al_2O_3$ catalyst (Fig. 9), a negative peak at 105 °C is attributed to the decomposition of palladium hydride.[29] The TPR profiles of

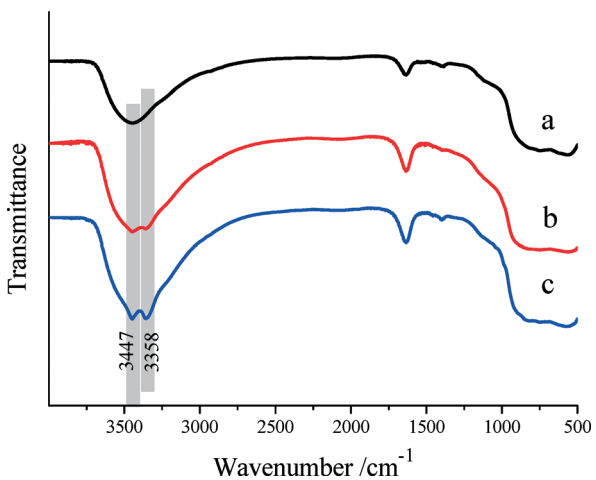

Fig. 7 FT-IR spectra of (a) Al_2O_3, (b) $Cu_2Cl(OH)_3/Al_2O_3$ (3.3 wt.% Cu) and (c) $Cu_2Cl(OH)_3/Al_2O_3$ (13.2 wt.% Cu).

$CuCl_2/Al_2O_3$ exhibits two reduction peaks at 280 °C and 360 °C. The former is related to the reduction of Cu^{2+} to Cu^+, and the latter results from the reduction of Cu^{2+} to Cu^0.[30]

There are two reduction peaks at 160 and 285 °C in the TPR profiles of the PCC-WI catalyst. The low temperature peak is related to the co-reduction of Pd and Cu species and the peak at 285 °C is ascribed to the reduction of isolated Cu species that have no interaction with the Pd species.[19] In the TPR profile of the PCC-CI catalyst, only one reduction peak at 130 °C could be observed, and this could be ascribed to the co-reduction of Pd and Cu species on the catalyst surface. The reduction peak of bulk Cu species could be observed at >180 °C.

The TPR profiles of the PCC-TI catalysts are very different from those of PCC-WI and PCC-CI. In the TPR profiles of the PCC-TI catalysts, two reduction peaks are located at 90–100 and 120 °C (Fig. 9). To clarify the attribution of the two reduction peaks of PCC-TI, samples with different Cu and Pd loadings were prepared for the TPR experiments. The results in Fig. 10A show that, with the increase of Cu loading in the Cu-1.7 wt.% Pd catalysts, the reduction peaks of PCC-TI/ethanol shifted to higher temperatures and the reduction peak area increased significantly. When the Cu loading was increased to 6.6 wt.% in the Cu-1.7 wt.% Pd sample, its γ peak appeared at 380 °C.

When the Cu loading was fixed to be 6.6 wt.%, with an increase in Pd loading in the PCC catalysts, the α peak shifted to lower temperatures and its reduction peak area increased gradually, but the γ peak was hardly changed (Fig. 10B). These results demonstrate that the sharp α peak could be related to the co-reduction of the Pd and Cu species on the catalyst surface, and the β peak might be associated with the reduction of surface Cu species near the Pd species, and the γ peak could be ascribed to the reduction of bulk Cu species. For the 6.6 wt.% Cu–0.8 wt.% Pd catalyst, its TPR curve is similar to that of the $CuCl_2/Al_2O_3$ sample and is different from those of the other 6.6 wt.% Cu–Pd catalysts, which shows that the presence of Pd promotes the reduction of Cu^{2+} ions and if the Pd loading is very low, this promotion of Pd would not be obvious. For the PCC-TI catalysts

Table 1 Compositions, surface areas (S_{BET}) and $Cu_2Cl(OH)_3$ sizes of PCC catalysts

Catalyst	In solution (wt.%)		In solid (wt.%)[a]		S_{BET} ($m^2\ g^{-1}$)	$Cu_2Cl(OH)_3$ size[b] (nm)
	Cu	Pd	Cu	Pd		
PCC-WI	3.3	1.7	3.24	1.57	126	34
PCC-CI	3.3	1.7	3.21	1.51	129	16
PCC-TI/methanol	3.3	1.7	3.19	1.58	137	19
PCC-TI/ethanol	3.3	1.7	3.15	1.57	139	17

[a] Determined by the ICP-OES method. [b] Calculated by the Scherrer equation based on the diffraction peak of the (101) facet of $Cu_2Cl(OH)_3$.

prepared by the two-step impregnation method with different alcohol solvents, their TPR curves are similar (Fig. 9), indicating that the reducibility of the PCC-TI catalyst is hardly affected by the alcohol solvent.

The results mentioned above show that the interaction between the copper and palladium species in the PCC-TI catalysts was stronger, and the presence of Pd can promote the reduction of Cu^{2+} ions, compared with the PCC-WI and PCC-CI catalysts. For the PCC-TI/ethanol prepared in the ethanol solvent, it possesses a lower reduction temperature (the maximum temperature of the α peak was 90 °C) and a stronger interaction between the Cu species and Pd species, that is, the α peak area of PCC-TI/ethanol is larger than that of PCC-TI/methanol, resulting in its higher catalytic activity for CO oxidation.

3.6. *In situ* DRIFTS of the surface reaction and the CO → CO_2 reaction at the Pd site

Fig. 11 shows the DRIFTS spectra of the catalysts in mixed gases containing 0.15% CO–20% O_2–3.1% H_2O/N_2. The absorption peaks at 2300–2400 cm^{-1} could be associated with the gaseous CO_2, the peaks at 1600–1700 cm^{-1} might be ascribed to –OH groups.[31,32] The peaks near 2110 cm^{-1} could be related with the Cu^+–CO complex, the peaks at 1930–1940 cm^{-1} may be assigned to bridged carbonyl ligands in Pd^+ complexes (Pd^+–CO), the weak peaks at 1990–2000 cm^{-1} are related to bridge-bonded CO on metallic palladium (Pd_2–CO), and the peaks at 2162 cm^{-1} are associated with terminal CO groups in Pd^{2+} complexes (Pd^{2+}–CO).[33,34] The strong peaks at 1822 cm^{-1} are related to triply bonded CO on metallic Pd (Pd_3–CO). The peaks at 1200–1600 cm^{-1} are associated with carbonate species.[35]

As shown in the IR spectra of the PCC-TI/ethanol catalyst (Fig. 11A), the intensities of the Pd_2–CO peak and Pd^+–CO peak decreased significantly, and the absorption peaks of Pd_3–CO, OH group and gaseous CO_2 increased gradually, with increasing reaction time.

The DRIFTS spectra of the PCC-CI catalyst are shown in Fig. 11B, the absorption peaks of the adsorbed CO (except Pd_3–CO) decreased significantly and the peaks of the adsorbed –OH groups increased gradually with increasing reaction time. Comparing with the IR spectra of the PCC-TI/ethanol catalyst, some differences can be found: traces of the Cu^+–CO peak were observed at the beginning of the reaction, but this peak could not be seen in the IR spectra of PCC-TI/ethanol, which demonstrates that the oxidation rate of the Cu^+ species on the PCC-CI surface was slower than that on PCC-TI/ethanol; the absorption bands of carbonates could be observed clearly and increased with the reaction time, which

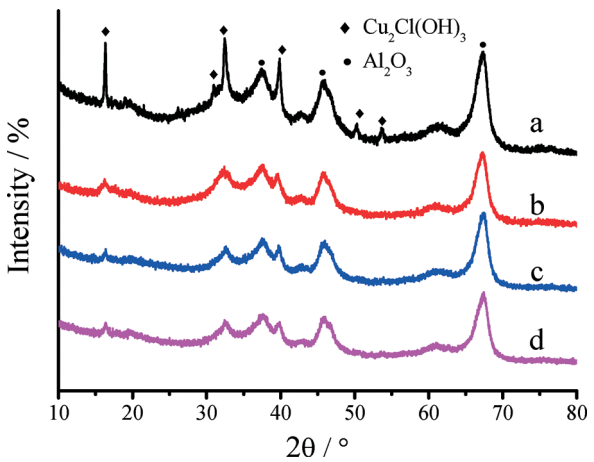

Fig. 8 XRD patterns of (a) PCC-WI, (b) PCC-CI, (c) PCC-TI/methanol, and (d) PCC-TI/ethanol.

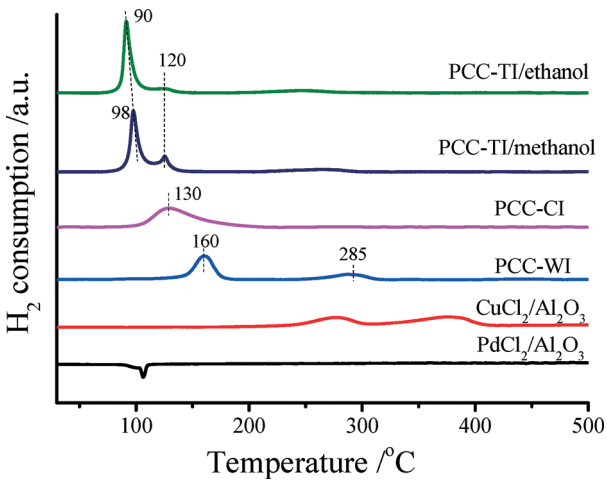

Fig. 9 TPR profiles of PCC-TI/ethanol, PCC-TI/methanol, PCC-CI, PCC-WI, $CuCl_2/Al_2O_3$ and $PdCl_2/Al_2O_3$ ($CuCl_2/Al_2O_3$ and $PdCl_2/Al_2O_3$ were prepared by the WI method in H_2O solvent).

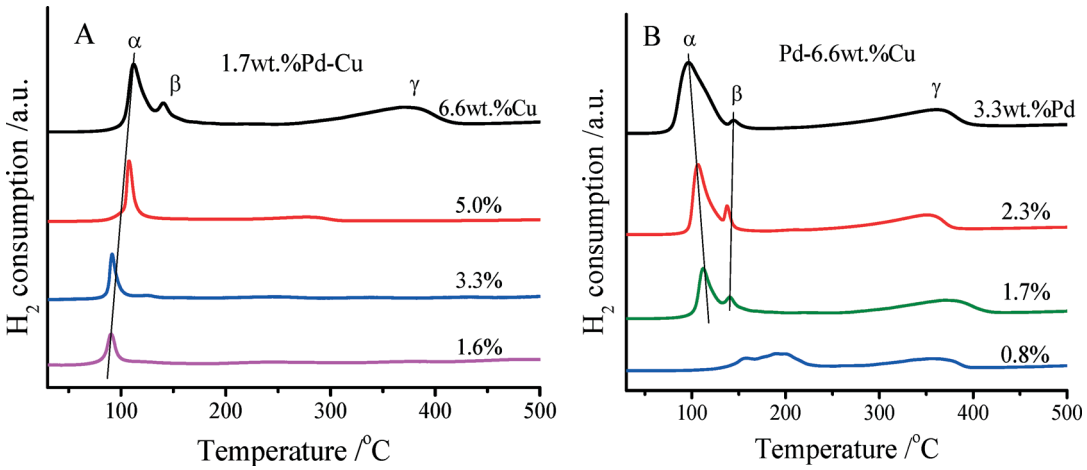

Fig. 10 TPR profiles of the PCC-TI/ethanol sample with (A) (1.6–6.6)wt.% Cu–1.7 wt.% Pd, and (B) 6.6 wt.% Cu–(0.8–3.3)wt.% Pd.

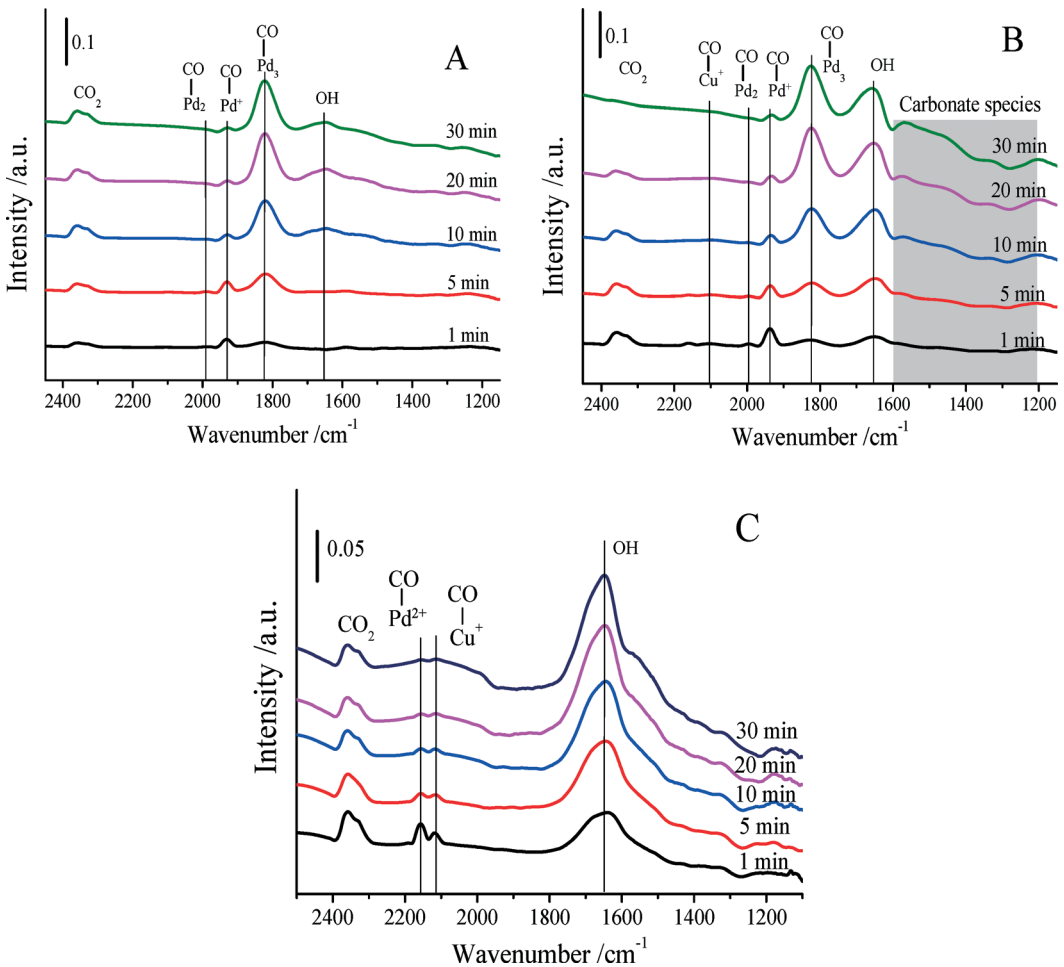

Fig. 11 *In situ* DRIFTS spectra of CO adsorbed over (A) PCC-TI/ethanol, (B) PCC-CI and (C) PCC-WI in a mixed gas containing 0.15% CO–20% O_2–3.1% H_2O/N_2 at 25 °C.

suggests the carbonate species was easily accumulated on the PCC-CI surface, resulting in the reduction of its catalytic activity and stability; and the absorption peak of gaseous CO_2 at 2300–2400 cm^{-1} declined gradually and disappeared with increasing reaction time, which shows that this catalyst has been deactivated for CO oxidation.

Being quite different from the IR spectra of the PCC-TI/ethanol and PCC-CI catalysts, in the IR absorption spectra of the PCC-WI catalyst (Fig. 11C), the IR absorption peaks corresponding to Cu^{+}–CO and Pd^{2+}–CO were present, and peaks corresponding to Pd^{+}–CO could not be observed. It was reported that the Pd^{+} sites have a higher activity than the Pd^{2+} sites for the CO oxidation, CO adsorbed on the Pd^{+} sites could be oxidized to CO_2 more easily than the CO adsorbed on the Pd^{2+} sites.[22] This is the reason that the PCC-TI/ethanol and PCC-CI catalysts exhibited a higher catalytic activity than the PCC-WI catalyst for CO oxidation.

Although there are differences in the DRIFTS spectra, as described above for CO oxidation over the Pd–Cu–Cl_x/Al_2O_3 catalysts prepared by the different methods, we would like to look at the similarities between them to understand the general catalytic mechanism. As shown in Fig. 10, –OH groups, metallic Pd^0(Pd_3–CO) and Pd^{+} complexes (Pd^{+}–CO) are common species in the catalytic oxidation process of CO. In our previous theoretical work, we studied the catalytic oxidation mechanism of CO on the Pd–Cu–Cl_x/Al_2O_3 catalyst. We found that the Pd centres are the main active sites for CO catalysis and the Cu centres are the main active sites for O_2 catalysis.[23] For Cu catalysis, O_2 was absorbed on Cu^{+} to form Cu^{2+}–O_2, and then the O atom was transferred to Pd^0–CO *via* a redox process, resulting in CO oxidation and the formation of a Pd^{+} species. More information can be obtained in ref. 23. For the process involving Pd centres as the active sites for CO catalysis, we used DFT calculations to further study the catalytic cycle of CO oxidation on the Pd species to reveal the possible routes for the formation of common species observed in the DRIFTS spectra. The main energy change and corresponding structures are shown in Fig. 12.

In the presence of –OH dissociated from H_2O, $PdCl_2$ is converted to Pd–OH (Fig. 12a). CO adsorbs onto PdOH to form the CO–Pd–OH species (Fig. 12b), which corresponds to the Pd^{+}–CO peak in the DRIFTS spectra, while this structure transforms into a *cis*-PdCOOH intermediate with an energy barrier of 0.52 eV (Fig. 12b). Next, the *cis*-PdCO–OH (Fig. 12d) directly dissociates –H to the nearest surface –OH to form adsorbed H_2O and Pd–CO_2, and then releases CO_2 to the gas phase (Fig. 12e), while Pd^0 is produced (Fig. 12f). After CO adsorption, Pd^0 transforms into Pd–CO (Fig. 12g) with an adsorption energy of 1.52 eV. The evidence for Pd^0 is shown by the CO–Pd_3 absorption peak at 1822 cm^{-1} in the DRIFTS spectra. These results show that the theoretical results are well correlated to the DRIFTS spectra, and mutually validate each other.

H_2O plays a subtle role in the CO catalytic oxidation over the Pd–Cu–Cl_x/Al_2O_3 catalyst. The DFT study showed that trace amounts of H_2O on a dry γ-Al_2O_3 surface could work as part of the catalytic cycle for low temperature CO oxidation, but when the moisture was excessive, the dissociated –H and –OH would occupy the Pd and Cu active sites on the Al_2O_3 surface as poisonous species, resulting in the deactivation of the catalyst for CO oxidation. The results of the DRIFTS study for the surface reaction show the intensities of the –OH groups on three catalysts prepared by different methods. The intensity of the –OH groups on the surface of PCC-TI/ethanol was weaker than that on PCC-WI and PCC-CI, which clearly confirms that moderate amounts of –OH groups are advantageous to CO oxidation, according to the results of the DFT study.

The DRIFTS results above also show that carbonate species hardly accumulated on the PCC-TI/ethanol catalyst, in which the oxidation rate of Cu^{+} to Cu^{2+} was faster than that in the PCC-CI catalyst, indicating that the PCC-TI/ethanol catalyst has better activity and stability than the other catalysts.

4. Conclusions

In summary, Pd–Cu–Cl_x/Al_2O_3 catalysts were prepared by three different preparation methods for low temperature CO oxidation. The PCC-TI catalysts prepared by the two-step impregnation (TI) method showed outstanding catalytic activities and stabilities compared with the PCC-WI and PCC-CI catalysts prepared by the wet impregnation (WI) and NH_3 coordination–impregnation (CI) methods, respectively. Among the four catalysts, the reaction temperature for 100% CO conversion was the lowest (only 10 °C) in the presence of ~3.1% moisture over the PCC-TI/ethanol catalyst and its E_a

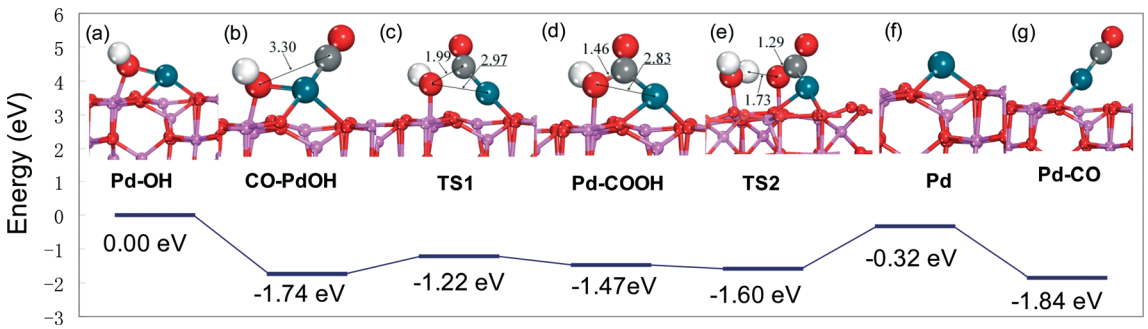

Fig. 12 The main energy change and corresponding structures for the catalytic cycle of the CO → CO_2 reaction on the Pd species. (a) Structure of Pd–OH, (b) structure of CO–PdOH, (c) transition state of the CO–PdOH → *cis*-PdCOOH reaction, (d) structure of *cis*-PdCOOH, (e) transition state of the *cis*-PdCOOH + –OH → Pd–CO_2 + –H_2O reaction, (f) adsorption state of Pd^0, and (g) structure of Pd–CO. (Bond lengths are reported in Å. O atoms are red, Al atoms are pink, H atoms are white, Al atoms are pink, and Pd atoms are dark blue).

was also the lowest (27.1 kJ mol^{-1}). The PCC-TI catalysts exhibited excellent catalytic activity, which could be ascribed to the higher dispersion of the $Cu_2Cl(OH)_3$ phase on its surface and the stronger interaction between copper and palladium species. For the PCC-TI catalysts, the solvent in the synthesis solution affected its catalytic performance. The PCC-TI/ethanol prepared in the ethanol solvent showed a higher activity than PCC-TI/methanol, which resulted from the much stronger interaction between the copper and palladium species.

The –OH groups on the Pd–Cu–Cl_x/Al_2O_3 catalyst surface played important roles in the catalytic oxidation of CO, moderate amounts of –OH groups can work as parts of the catalytic cycle as an important species for low temperature CO oxidation, and excessive –OH groups could occupy the active sites on the Al_2O_3 surface, resulting in a deactivation of the catalyst. Compared with the PCC-CI catalyst, carbonate species are hardly accumulated on the PCC-TI/ethanol surface, which results in higher stability. High CO concentration played a negative influence on the CO conversion, and may originate from the competitive adsorption and the covering of carbonates on the catalyst surface. We used DFT calculations to study the catalytic cycle of CO oxidation on the Pd species to reveal the possible routes for formation of common species observed in the DRIFTS spectra.

Acknowledgements

This project was financially supported by the National Natural Science Foundation of China (21273150, 21203119), the National Basic Research Program of China (2013CB933201), the national high technology research and development program of China (2011AA03A406, 2012AA062703), the Shanghai Natural Science Foundation (12ZR1430800), and the Shanghai Innovation Program (12YZ161).

Notes and references

1 M. Chen and D. Goodman, *Science*, 2004, **306**, 252.
2 C. Jones, S. H. Taylor, A. Burrows, M. J. Crudace, C. J. Kiely and G. J. Hutchings, *Chem. Commun.*, 2008, 1707.
3 J. Y. Luo, M. Meng, X. Li, X. G. Li, Y. Q. Zha, T. D. Hu, Y. N. Xie and J. Zhang, *J. Catal.*, 2008, **254**, 310.
4 X. Xie, Y. Li, Z. Q. Liu, M. Haruta and W. Shen, *Nature*, 2009, **458**, 746.
5 Y. Yu, T. Takei, H. Ohashi, H. He, X. Zhang and M. Haruta, *J. Catal.*, 2009, **267**, 121.
6 D. R. Merrill and C. C. Scalione, *J. Am. Chem. Soc.*, 1921, **43**, 1982.
7 F. Grillo, M. M. Natile and A. Glisenti, *Appl. Catal., B*, 2004, **48**, 267.
8 E. C. Njagi, C. H. Chen, H. Genuino, H. Galindo, H. Huang and S. L. Suib, *Appl. Catal., B*, 2010, **99**, 103.
9 M. Haruta, N. Yamada, T. Kobayashi and S. Iijima, *J. Catal.*, 1989, **115**, 301.
10 G. Y. Wang, H. L. Lian, W. X. Zhang, D. Z. Jiang and T. H. Wu, *Kinet. Catal.*, 2002, **43**, 433.
11 J. M. Soares, M. Hall, M. Cristofolini and M. Bowker, *Catal. Lett.*, 2006, **109**, 103.
12 I. D. Gómez, I. Kocemba and J. M. Rynkowski, *Appl. Catal., B*, 2009, **88**, 83.
13 S. H. Choi and J. S. Lee, *React. Kinet. Catal. Lett.*, 1996, **57**, 227.
14 J. S. Lee, S. H. Choi, K. D. Kim and M. Nomura, *Appl. Catal., B*, 1996, **7**, 199.
15 E. D. Park and J. S. Lee, *J. Catal.*, 1998, **180**, 123.
16 E. D. Park, S. H. Choi and J. S. Lee, *J. Phys. Chem. B*, 2000, **104**, 5586.
17 E. D. Park and J. S. Lee, *J. Catal.*, 2000, **193**, 5.
18 A. J. Dyakonov, *Appl. Catal., B*, 2003, **45**, 257.
19 Y. Shen, G. Lu, Y. Guo and Y. Wang, *Chem. Commun.*, 2010, **46**, 8433.
20 L. Wang, Y. Zhou, Q. Liu, Y. Guo and G. Lu, *Catal. Today*, 2010, **153**, 184.
21 Y. Shen, Y. Guo, L. Wang, Y. Wang, Y. Guo, X. Gong and G. Lu, *Catal. Sci. Technol.*, 2011, **1**, 1202.
22 Y. Shen, G. Lu, Y. Guo, Y. Wang, Y. Guo and X. Gong, *Catal. Today*, 2011, **175**, 558.
23 C. Shen, H. Li, J. Yu, G. Wu, D. Mao and G. Lu, *ChemCatChem*, 2013, **5**, 2813.
24 W. Wei, P. Gao, J. Xie, S. Zong, H. Cui and X. Yue, *J. Solid State Chem.*, 2013, **204**, 305.
25 G. Kresse and D. Joubert, *Phys. Rev. B: Condens. Matter Mater. Phys.*, 1999, **59**, 1758.
26 M. Digne, P. Sautet, P. Raybaud, P. Euzen and H. Toulhoat, *J. Catal.*, 2004, **226**, 54.
27 K. D. Kim, I. S. Nam, J. S. Chung, J. S. Lee, S. G. Ryu and Y. S. Yang, *Appl. Catal., B*, 1994, **5**, 103.
28 D. J. Koh, J. H. Song, S. W. Ham, I. S. Nam, R. W. Chang, E. D. Park, J. S. Lee and Y. G. Kim, *Korean J. Chem. Eng.*, 1997, **14**, 486.
29 W. J. Shen, M. Okumura, Y. Matsumura and M. Haruta, *Appl. Catal., A*, 2001, **213**, 225.
30 A. Rouco, *J. Catal.*, 1995, **157**, 380.
31 H. Zhu, Z. Qin, W. Shan, W. Shen and J. Wang, *J. Catal.*, 2004, **225**, 267.
32 H. Zhu, Z. Qin, W. Shan, W. Shen and J. Wang, *J. Catal.*, 2005, **233**, 41.
33 K. I. Choi and M. A. Vannice, *J. Catal.*, 1991, **127**, 489.
34 K. I. Choi and M. A. Vannice, *J. Catal.*, 1991, **131**, 22.
35 O. Pozdnyakova, D. Teschner, A. Wootsch, J. Kröhnert, B. Steinhauer, H. Sauer, L. Toth, F. Jentoft, A. Knop-Gericke and Z. Paál, *J. Catal.*, 2006, **237**, 1.